JOURNAL OF PROPULSION AND POWER
Vol. 18, No. 3, May–June 2002

Multiobjective Optimization of Rocket Engine Pumps Using Evolutionary Algorithm

Akira Oyama* and Meng-Sing Liou†
NASA John H. Glenn Research Center at Lewis Field, Cleveland, Ohio 44135

A design optimization method for turbopumps of cryogenic rocket engines has been developed. Multiobjective evolutionary algorithm is used for multiobjective pump design optimizations. Performances of design candidates are evaluated by using the meanline pump flow-modeling method based on the Euler turbine equation coupled with empirical correlations for rotor efficiency. To demonstrate feasibility of the present approach, single-stage centrifugal pump and multistage pump design optimizations are performed. The number of pump performance evaluations necessary to obtain a reasonable pareto-optimal set for the conceptual rocket engine pump design will be investigated using the single-stage centrifugal pump design optimization. In both design optimizations the present method obtains hundreds of reasonable and uniformly distributed pareto-optimal solutions that include some designs outperforming the original design in total head while reducing input power by 1%. Detailed observation of the design results also reveals some important design criteria for turbopumps in cryogenic rocket engines. These results demonstrate the feasibility of the evolutionary algorithm-based multiobjective design optimization method in this field.

I. Introduction

ALTHOUGH budget for space development programs has drastically shrunk in most countries, recent and future space missions increasingly demand high performance and reliable rocket engine systems and components, such as turbopumps. Progress in computational fluid dynamics (CFD) methods and development of powerful computational facilities have contributed to the reduction in required cost and time to develop advanced turbopump designs. The design process still largely depends on experienced designers. Therefore, numerical design methods coupled with CFD, which are capable of efficiently developing advanced turbopump designs, can greatly reduce such dependency.

Yet, despite the fact that numerical optimization methods have been successfully applied to a variety of design problems, application of numerical optimization method to rocket engine pump design still remains as a formidable challenge. One of the main reasons is that a rocket engine pump design involves simultaneous optimization of multiple and competing objectives such as maximization of total head rise, minimization of input power, minimization of weight, etc. Although single-objective optimization problems might have a unique optimal solution, multiobjective problems (MOPs) present a set of compromised solutions, largely known as the tradeoff surface, pareto-optimal solutions or nondominated solutions.[1] These solutions are optimal in the sense that no other solutions in the search space are superior to them when all objectives are considered (Fig. 1). The goal of MOPs is to find as many pareto-optimal solutions as possible to reveal tradeoff information among different objectives. Once such solutions are obtained, the higher-level decision-maker will be able to choose a final design with further considerations.

Received 23 July 2001; revision received 16 November 2001; accepted for publication 19 November 2001.

*NRC Research Associate, Ohio Aerospace Institute ICOMP, 22800 Cedar Point Road, Cleveland, OH 44142.

†Senior Scientist, MS 5-11; meng-sing.liou@grc.nasa.gov.

Traditional design methods such as the gradient-based methods[2,3] are single-objective optimization methods that optimize one objective. These methods usually start with a single baseline design and use local gradient information of the objective function with respect to changes in the design variables to calculate a search direction. When these methods are applied to a MOP, the problem is usually transformed into a single-objective optimization problem by combining multiple objectives into a single objective typically using a weighted sum method. For example, to minimize competing functions f_1 and f_2 these objective functions are combined into a scalar function F as

$$F = w_1 \cdot f_1 + w_2 \cdot f_2, \qquad w_1 + w_2 = 1 \tag{1}$$

This approach, however, can find only one of the pareto-optimal solutions corresponding to each set of the weights w_1 and w_2. Therefore, one must run many optimizations by trial and error adjusting the weights to get pareto-optimal solutions uniformly over the potential pareto-front. This is considerably time consuming in terms of human time. What is more, there is no guarantee that uniform pareto-optimal solutions can be obtained. For example, when this approach is applied to a MOP that has concave tradeoff surface it converges to two extreme optimums without showing any tradeoff information between the objectives (Fig. 2).

Evolutionary algorithms [(EAs) for example, see Ref. 4], on the other hand, are particularly suited for MOPs. By maintaining a population of design candidates and using a fitness assignment method based on the pareto-optimality concept, they can uniformly sample various pareto-optimal solutions in one optimization without converting a MOP into a single-objective problem. In addition, EAs have other advantages such as robustness, efficiency, as well as suitability for parallel computing. Because of these advantages, EAs are a unique and attractive approach to real-world design optimization problems such as the rocket engine pump design optimization problem. Recently, EAs have been successfully applied to aerospace design optimization problems.[4–8]

The objective of the present study is to develop and demonstrate a design optimization method for turbopumps used in the cryogenic rocket engines. The multiobjective evolutionary algorithm (MOEA) will be used for multiobjective optimization of pump designs. Performances of design candidates will be evaluated by using the meanline pump flow-modeling method based on the Euler turbine equation coupled with empirical correlations for rotor efficiency. The present approach will be applied to conceptual designs of centrifugal and multistage turbopumps.

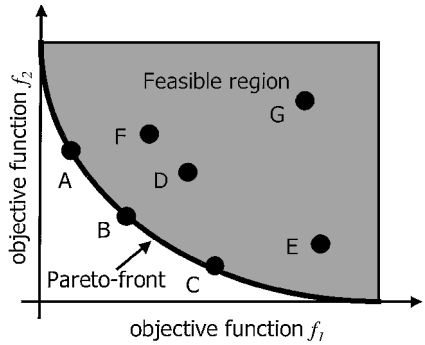

Fig. 1 Concept of pareto-optimality. This is an example of MOPs, which minimizes two conflicting objectives f_1 and f_2. This MOP has innumerable compromised pareto-optimal solutions such as solutions A, B, and C. These solutions are optimal in the sense that there is no better solution in both objectives. One cannot say which is better among these pareto-optimal solutions because improvement in one objective degrades another.

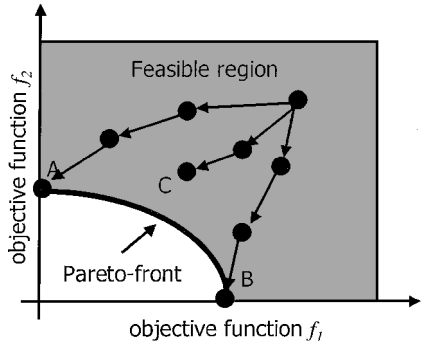

Fig. 2 Weighted sum method applied to a MOP having a concave pareto-front. Any combination of weights w_1 and w_2 would result in the extreme optimum A or B. A gradient-based method might stack in a local optimum C because of complexity of the objective function distributions.

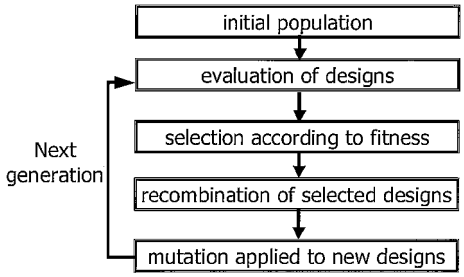

Fig. 3 Flowchart of the present evolutionary algorithm.

II. Evolutionary Algorithms

EAs mimic mechanisms of natural evolution, where a biological population evolves over generations to adapt to an environment by selection according to fitness, recombination, and mutation of genes (Fig. 3). In EAs a design candidate, objective function values, and design variables usually correspond to an individual, fitness, and genes, respectively.

Starting with an initial population of design candidates that is often generated by random sampling from the design space, EAs select good design candidates in terms of fitness, which is assigned on the bias of their objective function values. Typically, fitness of a design candidate is its objective function value itself for a single-objective problem. For a MOP an individual's fitness is determined according to pareto-optimal concept.[1] Recombination is applied, where new population is generated by exchanging features of the selected designs with the intent of improving the fitness of the next generation. Then, mutation is applied to design parameters of the new population to maintain diversity in the population. EAs for MOPs are called MOEAs.[4]

One of the key features of EAs is that it searches from multiple points in the design space in contrast to the traditional methods that usually move from a single design point. In addition, EAs use objective function values alone to determine a search direction and do not require derivatives or gradients of the objective function while the traditional methods use local gradient information of an objective function. These features also lead to some advantages such as the following:

1) The first advantage is the capability of sampling various pareto-optimal solutions in parallel. By maintaining a population of solutions and introducing the concept of pareto-optimality for fitness assignment, EAs can uniformly sample various pareto-optimal solutions in parallel when applied to MOPs.

2) The second advantage is robustness. Deterministic methods such as the gradient-based methods typically start with a single design point and use the local gradient information to determine a search direction. Optimization depending on such local information leads to a local, not necessarily a global, optimum nearby the stating point. In contrast to them, EAs determine their search direction globally and probabilistically but efficiently using their unique operators so-called recombination and mutation that give EAs capability of finding global optimums. Compared with other probabilistic methods such as the simulated annealing method[3] that is similar to the gradient-based methods but tries random step according to the so-called Boltzmann probability distribution, EAs are more robust because they maintain a population of design candidates, and they do not use function gradients that direct the search toward a local optimum. In addition, EAs have capability to handle any design problems that might involve nondifferentiable objective function and/or a mix of continuous, discrete, and integer design parameters.

3) Suitability to parallel computing is the third advantage. Because EAs are population-based search algorithms, all design candidates in each generation can be evaluated in parallel by using a simple master-slave concept. Parallel efficiency is extremely high, if objective function evaluations consume most of CPU time.

4) Simplicity in coupling evaluation codes is the fourth advantage. Because EAs use only objective function values of design candidates, EAs do not need substantial modification or sophisticated interface to evaluation codes. If an all-out recoding were required to every optimization problem, extensive validation of the new code would be necessary every time. EAs can save such troubles.

The present MOEA uses floating-point representation, where an individual is characterized by a vector of real numbers. It is natural to use the floating-point representation for real parameter optimization problems instead of binary representation because it is conceptually closest to the real design space, and moreover, the string length is reduced to the number of design variables.

To introduce the pareto-optimality concept to the present MOEA, Fonseca's pareto-based ranking method[9] is used for fitness assignment where an individual's rank corresponds to the number of individuals in the current population who are better than the corresponding individual in every objective function. Fonseca's ranking method for a minimization problem is shown in Fig. 4. Then, the N best individuals are selected from both the present N design candidates and the previous N design candidates for mating pool according to their ranks where populations size is set equal to N (see Ref. 10). A standard sharing function[11] is incorporated to maintain diversity in the population.

To generate new design candidates, the blended crossover (BLX-α) is applied to the best N individuals, where mating is determined randomly. The blended crossover is the most common approach for recombination of two parents represented by a vector of real numbers proposed by Eshelman and Schaffer.[12] In this approach children are generated on a segment defined by two parents, but the segment can be extended equally on both sides determined by a user-specified parameter α. Thus, a child solution is expressed as

$$\text{Child } 1 = \gamma \cdot \text{Parent } 1 + (1 - \gamma) \cdot \text{Parent } 2 \tag{2}$$

$$\text{Child } 2 = (1 - \gamma) \cdot \text{Parent } 1 + \gamma \cdot \text{Parent } 2 \tag{3}$$

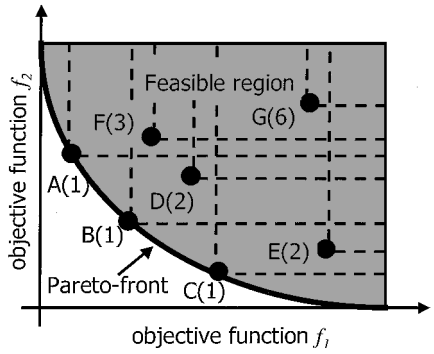

Fig. 4 Fonseca's pareto-ranking method for a multiobjective minimization problem. The solutions A, B, C rank first because they are pareto-optimal. The solutions D and E rank second because they are worse than the solutions B and C on both objectives, respectively. The solution F ranks third because two solutions (A and B) are better than the solution F on both objectives.

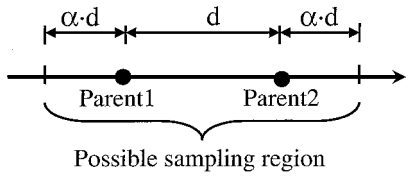

Fig. 5 Blended crossover.

where

$$\gamma = (1 + 2\alpha)u - \alpha \tag{4}$$

Child 1, Child 2 and Parent 1, Parent 2 denote design parameters of the children and parents, respectively; u is uniform random number in [0, 1]. Schematic view of BLX-α is shown in Fig. 5. When an EA is applied to a design optimization problem, what is important is the balance of two conflicting goals: exploiting good solutions and exploring the search space.[13] Thus, BLX-0.5 is used in which both exploration and exploitation are carried out equally. Because the strong elitism is used, high mutation rate of 0.2 is applied, and a random disturbance is added to the parameter in the amount up to ±20% of the design space. Unbiased initial population is generated by randomly spreading solutions over the entire design space in consideration.

III. Pump Performance Evaluation

Total head and required input power of pump design candidates are evaluated by using a one-dimensional meanline pump flow-modeling method,[14] which provides a fast capability for modeling turbopumps within rocket engines. This method has been validated by simulating a variety of very different pumps such as Mark48 liquid hydrogen pump, XLR-129 liquid hydrogen pump, Orbital Transfer Vehicle liquid oxygen pump, etc.

The components of the inlet and exit fluid velocity triangles are calculated at the hub, mean, and tip locations along the rotor blades. The meridional velocity of the fluid at the rotor leading-edge rms diameter C_{M1} (m/s) is defined by Eq. (5):

$$C_{M1} = m/\rho_1 A_1 \tag{5}$$

where m is the mass flow (kg/s), ρ_1 the fluid density at leading edge (kg/m^3), A_1 the flow area at leading edge (m^2).

Flow area is calculated from the input flow path dimensions:

$$A = \lambda \lfloor \pi B(R_{\text{hub}} + R_{\text{tip}}) - \text{block} \rfloor \tag{6}$$

where λ is the boundary-layer blockage factor, B the blade span from hub to tip (m), R_{hub} the radial distance from pump centerline at hub (m), R_{tip} the radial distance from pump centerline at tip (m).

The metal blockage of the rotor block is calculated by Eq. (7):

$$\text{block} = \frac{thk \cdot B \cdot Z}{\sin\beta} \tag{7}$$

where thk is the normal blade thickness (m), Z the blade number, and β the relative angle from tangential, deg.

The tangential component of velocity entering the rotor is calculated in terms of the swirl angle of the flow α_1 by Eq. (8):

$$C_{U1} = \frac{C_{M1}}{\tan(\alpha_1)} \tag{8}$$

The meridional and tangential components of absolute fluid velocity at the rotor trailing edge are calculated by Eqs. (9) and (10):

$$C_{M2} = m/\rho_2 A_2 \tag{9}$$

$$C_{U2} = U_2 + W_{U2} \tag{10}$$

where ρ_2 is the fluid density at trailing edge (kg/m^3), A_2 the flow area at trailing edge (m^2), U_2 the blade tangential velocity at trailing edge (m/s), and W_{U2} the tangential component of relative fluid velocity at trailing edge (m/s).

Flow area at trailing edge is calculated by Eq. (6). The blade tangential velocity U and tangential component of the fluid relative velocity W_{U2} are given by Eqs. (11) and (12), respectively:

$$U = \frac{2\pi \cdot R \cdot N}{60} \tag{11}$$

$$W_{U2} = C_{M2} \cdot \tan\beta_2 + U_2(1 - \sigma) \tag{12}$$

where R is the radial distance from pump centerline (m), N the shaft rotative speed (rpm), and β_2 the relative angle from tangential at trailing edge (deg).

The slip factor σ is defined by

$$\sigma = 1 - \text{slip}/U_2 \tag{13}$$

The slip is the difference between the theoretical and absolute fluid tangential velocities. For centrifugal impellers Pfleiderer correlation to geometry[15] is used to calculate the slip factor σ. A default slip factor of 0.95 is used for inducers.

The head rise through the rotor is calculated iteratively from the Euler turbine equation coupled with empirical correlations for rotor efficiency

$$H_2 = [(U_2 \cdot C_{U2} - U_1 \cdot C_{U1})/g_c] \cdot \eta_{\text{hyd}} \tag{14}$$

where H_2 is the head rise through the rotor (m), η_{hyd} the rotor hydraulic efficiency; and g_c the gravitational constant, 9.8 m/s^2.

The rotor hydraulic efficiency is obtained from empirical correlations to rotor-specific speed.[16] The total pressure and static pressure at the rotor exit are estimated from the rotor head rise by Eqs. (15) and (16):

$$P_{t2} = H_2 \cdot \rho_{1-2} + P_{t1} \tag{15}$$

$$P_{s2} = P_{t2} - \frac{C_2^2 \cdot \rho_2}{2 \cdot g_c} \tag{16}$$

where P_{t1} is the total pressure at the leading edge (kgf/m^2), P_{t2} the total pressure at the trailing edge (kgf/m^2), ρ_{1-2} the average density of the fluid from the leading edge to the trailing edge (kg/m^3), and P_{s2} the static pressure at the trailing edge (kgf/m^2).

Fluid absolute velocity at trailing edge C_2 (m/s) is defined by

$$C_2 = \sqrt{C_{M2}^2 + C_{U2}^2} \tag{17}$$

Total pressure at the discharge of the last stage P_{t4} (kgf/m^2) is given by the following equation:

$$P_{t4} = P_{t2} - \omega_{2-4} \cdot (P_{t2} - P_{s2}) \tag{18}$$

where the total pressure loss coefficient of the diffusion system ω_{2-4} is a empirically derived function of loading parameter L[14]

$$\omega_{2-4}/\omega_{2-4,0} = 1.8151 - 1.83527 \cdot L + 0.8798 \cdot L^2 + 0.18765 \cdot L^3 \tag{19}$$

where the total pressure loss coefficient of the baseline diffusion system $\omega_{2-4,0}$ is assumed to be known. The loading parameter is defined in terms of the velocities at the vaneless diffuser exit and the velocity at the diffusion system throat.

$$L = \frac{C_{\text{throat}}}{\sqrt{C_{U3}^2 + C_{M3}^2}} \tag{20}$$

where C_{throat} is the fluid absolute velocity at the diffusion system throat (m/s), C_{U3} the tangential component of fluid absolute velocity at vaneless diffuser exit (m/s), and C_{M3} the meridional component of fluid absolute velocity at vaneless diffuser exit (m/s).

The velocity at the diffusion system throat is defined by the Eqs. (21) and (22).

$$C_{M3} = m/\rho_3 A_3 \tag{21}$$

$$C_{U3} = (1 - \omega_{2-3}) \cdot C_{U2} \cdot (R2/R3) \tag{22}$$

where the pressure loss coefficient at the diffuser exit ω_{2-3} is assumed to be 0.1. Fluid velocity at the throat is given by the Eq. (23):

$$C_{\text{throat}} = \frac{m}{\rho_3 A_{\text{throat}}} \tag{23}$$

The total head rise through pump is calculated by

$$H_4 = \frac{\cdot(P_{t4} - P_{t1})}{\rho_{1-4}} \tag{24}$$

where H_4 is the total head rise through pump (m), P_{t4} the total pressure at the pump exit (kgf/m^2), and ρ_{1-4} the average density of the fluid from the inlet to the discharge (kg/m^3).

The input power required to drive the rotor is calculated from the head rise through the rotor, mass flow, rotor hydraulic efficiency, mechanical efficiency, volumetric efficiency, and disk pumping loss as

$$\text{input} = \left(\frac{m \cdot H_2}{\eta_{\text{hyd}} \cdot \eta_{\text{vol}}} + PL_{\text{disk}} \right) \cdot \frac{1}{\eta_{\text{mech}}} \tag{25}$$

where input is the input power (kgf $\cdot$ m/s), η_{mech} the mechanical efficiency, η_{vol} the volumetric efficiency, and PL_{disk} the disk pumping loss (kgf $\cdot$ m/s).

The mechanical efficiency is assumed to be 0.98, and the volumetric efficiency is based on internal leakage and is expressed as the ratio of leakage to the inlet flow. The disk pumping loss is calculated from empirical correlations to geometry, fluid density at rotor trailing edge, and the shaft rotative speed.[15] During the calculation, local static pressure at the rotor tip is compared to the local vapor pressure to check for the cavitation inception point.

To compare overall performance maps of the baseline designs and pareto-optimal designs, off-design total head and required input power are estimated by using the empirically derived variation of slip factor and rotor efficiency as a function of flow-speed ratio F.[14,17]

$$\frac{\sigma}{\sigma_{\text{design}}} = 1.534988 - 0.6681688 \cdot F + 0.077472 \cdot F^2 + 0.0571508 \cdot F^3 \tag{26}$$

$$\frac{\eta_{\text{hyd}}}{\eta_{\text{hyd,design}}} = 0.86387 + 0.3096 \cdot F - 0.14086 \cdot F^2 - 0.029265 \cdot F^3 \tag{27}$$

IV. Centrifugal Pump Design

First, redesign of a single-stage centrifugal pump, M-1 oxygen $\frac{3}{8}$-scale water tester[18] is demonstrated.

A. Design Problem Formulation

Objectives of the present design problem are maximization of total head and minimization of input power at a design point. These objectives are competing, and therefore the solution to this optimization problem is pareto-optimal solutions.

The design point is shaft rotative speed of 5416.7 rpm, total temperature of the fluid entering the pump of 29.6°C, total pressure of the fluid entering the pump of 35200 kgf/m^2, and mass flow into the pump of 85.67 kg/s.

Design parameters are rotor leading-edge tip radius R_{tip1}, rotor trailing-edge radius R_2, volute tongue radius R_3, blade span at trailing edge B_2, blade span at volute tongue B_3, axial length of the blade at the rms diameter S, number of blades Z_n, blade thickness thk, blade trailing-edge angle at the hub, rms radius, and tip (β_{hub}, β_{mid}, β_{tip}) as shown in Fig. 6. Table 1 presents present design spaces.

B. Number of Evaluations Required for the Multiobjective Design

For EAs some parameters must be specified by users such as population size, number of generations, crossover rate, and mutation rate. Among them, populating size and number of generations are of great importance because they directly affect computational time as well as an EA's robustness. For example, optimization with large population size and large number of generations (that is, large number of evaluations) might always result in global optimal solutions, but it might require tremendous computational time. However, there is no research investigating how many evaluations are required for a multiobjective optimization as far as the authors know. Therefore, required number of evaluations for the present multiobjective optimization problem is examined in this section.

For a singleobjective optimization problem usually there is a unique optimum, and the convergence is easily examined using its objective function value. In contrast to that, a multiobjective optimization problem has pareto-optimal solutions, which have multiple objectives. Some metrics have been presented to compare some pareto fronts.[19–22] In this study generational distance G[23] is used as a measure of error of a current pareto front PF_{current} from the true pareto-front PF_{true}:

$$G = \frac{\sqrt{\sum_{i=1}^{n} d_i^2}}{n} \tag{28}$$

where n is the number of designs in PF_{current} and d_i is a distance between a design point ($f_{1,i}$, $f_{2,i}$, ...) in PF_{current} and the nearest point ($F_{1,j}$, $F_{2,j}$, ...) in PF_{true} in the objective function space given by

$$d_i = \sqrt{\sum_{k=1}^{m} (F_{k,j} - f_{k,i})} \tag{29}$$

where m is the number of objective functions. In this study PF_{true} is derived from five pareto-optimal fronts obtained by executing five optimizations using the EA with population size of 400 and 300 generations.

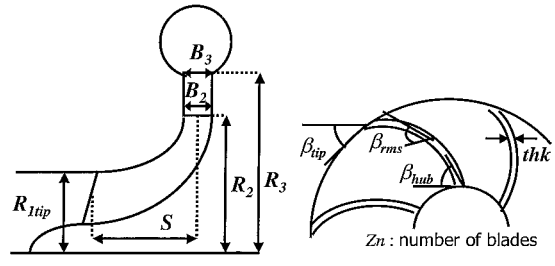

Fig. 6 Design parameters of the centrifugal pump design problem.

Table 1 Design parameter ranges of the centrifugal pump design problem

Design variables	$R_{1\,tip}$, in.	R_2, in.	R_3, in.	B_2, in.	B_3, in.	S, in.	β_{hub}, deg	β_{rms}, deg	β_{tip}, deg	thk_2, in.	Z_{n2}
Upper boundary	4.00	5.60	6.20	0.85	1.00	4.30	45.0	45.0	45.0	0.10	30
Lower boundary	3.40	5.00	5.60	0.70	0.85	3.70	25.0	25.0	25.0	0.03	4

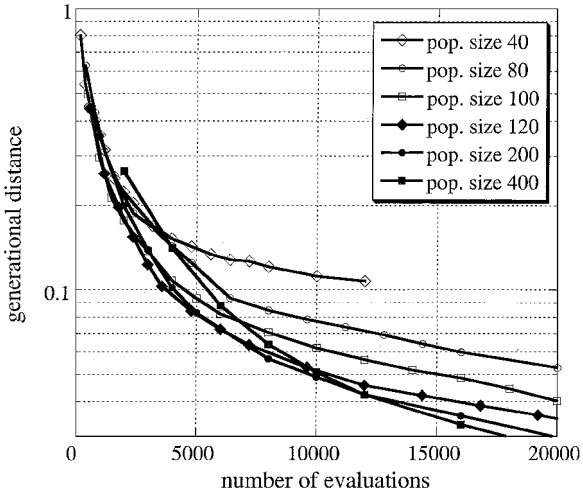

Fig. 7 Generational distance histories.

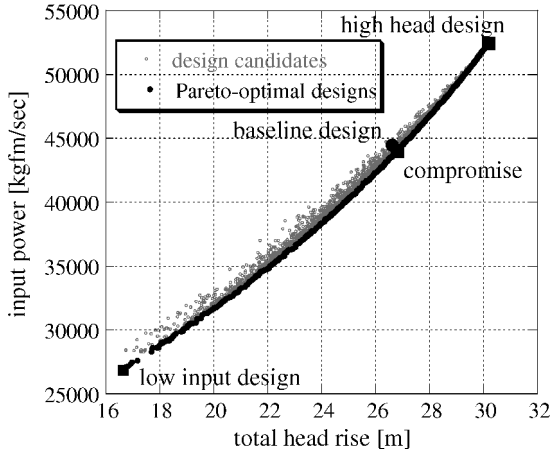

Fig. 8 Objective function values of the centrifugal pump designs.

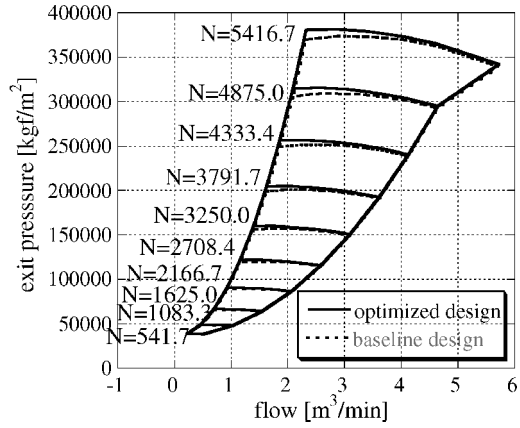

Fig. 9 Centrifugal pump overall performance map.

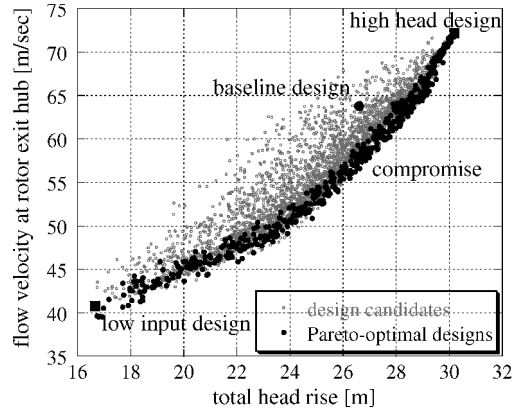

Fig. 10 Flow velocity at blade exit hub of the centrifugal pump designs.

Figure 7 shows the generational distance histories of optimizations with six different population sizes in terms of the number of evaluations. Each curve represents average of five optimizations starting with different initial populations. Examining some pareto-optimal fronts at different generational distance values, generational distance of 0.1 is assumed to be sufficient for the present problem. According to the figure, EA with population size of 100–200 worked efficiently for the current optimization problem. Among them EA with population size of 120 converged to generational distance of 0.1 with about 3000 evaluations that correspond to 25th generation.

C. Results

Next, pareto-optimal solutions of an optimization with population size of 120 at 30th generation are examined. An execution of EA obtained 498 different pareto-optimal solutions showing the tradeoff information among competing objectives. Though EAs are sometimes criticized because they require too large a number of evaluations, they require reasonable number of evaluations per an optimum when applied to a MOP. In the present case, the EA required about seven evaluations per an optimum (120 designs $\times$ 30 generations/498 optimums = 7.22). In this sense, EAs are very efficient.

Total head and input power of pareto-optimal designs, original design, and all other design candidates are illustrated in Fig. 8. Designs that have cavitation are eliminated from the figure. Present pareto-optimal solutions successfully display tradeoff information between maximization of the total head and minimization of the input power. Such tradeoff information is very helpful to a higher-level decision maker in selecting a design with other considerations. Among the pareto-optimal solutions, some designs outperform the original design in the total head while reducing the input power by 1%.

Figure 9 compares overall performance maps of the original design and a compromised design that overcomes the original design in both objectives. The compromised design improved the exit pressure in all off-design conditions. The design parameters of these designs are shown in Table 2.

The absolute flow velocity at rotor exit hub is shown in Fig. 10. This figure indicates the pareto-optimal designs have small exit flow velocity, which contributes to minimization of the total pressure loss in the diffusion system. By minimizing the total pressure loss in the diffusion system, designs can improve their total head rise. To minimize the exit flow velocity, the optimum designs have small slip factor values (that is, large slip than others). In fact, the high head design and the compromised design maximize R_2 to increase slip caused by the inertial effect while the low input design minimizes R_2 to minimize input power. The low input design and the compromised design also have small blade angle at hub and tip to reduce absolute fluid velocity at rotor exit while the high head design maximizes blade trailing-edge angles to improve its total head. However, it is

Table 2 Pareto-optimal designs of the centrifugal pump design problem

Design variables	$R_{1\,\mathrm{tip}}$, cm	R_2, cm	R_3, cm	B_2, cm	B_3, cm	S, cm	β_{hub}, deg	β_{rms}, deg	β_{tip}, deg	thk, cm	Z_n
High head design	9.80	14.2	14.6	2.08	2.21	10.6	43.3	35.9	44.2	0.211	13
Compromised design	8.84	14.2	14.4	1.78	2.49	10.1	27.5	37.3	28.1	0.249	7
Low input design	8.64	12.8	14.5	1.96	2.39	9.55	31.6	38.2	25.9	0.140	4
Original design	9.30	13.6	15.0	2.06	2.31	10.2	35.0	35.0	35.0	0.127	12

Table 3 Design parameter ranges of the multistage pump design problem

First stage						
Design variables	R_{tip}, cm	$R_{2\,\mathrm{hub}}$, cm	$\beta_{2\,\mathrm{hub}}$, deg	$\beta_{2\,\mathrm{rms}}$, deg	$\beta_{2\,\mathrm{tip}}$, deg	thk_2, cm	Z_{n2}
Upper boundary	3.00	1.35	50.0	40.0	35.0	0.203	10
Lower boundary	2.74	1.09	35.0	25.0	20.0	0.0762	2

Second stage							
Design variables	R_2, cm	$(R_4 - R_3)$, cm	B_2, cm	B_3, cm	thk_3, cm	S, cm	Z_{n3}	β_3, deg
Upper boundary	5.59	0.381	0.889	1.27	0.203	2.54	18	90.0
Lower boundary	5.08	0.127	0.381	0.762	0.0762	2.03	6	60.0

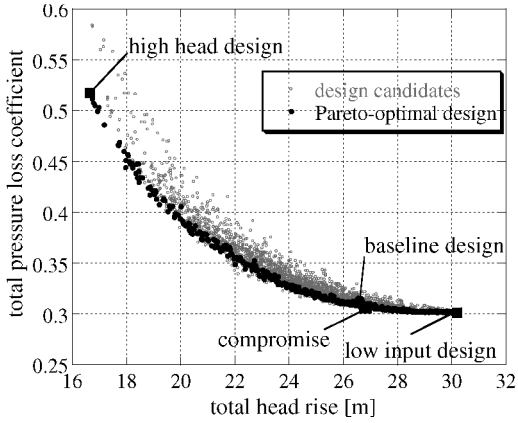

Fig. 11 Total pressure loss coefficient of the centrifugal pump designs.

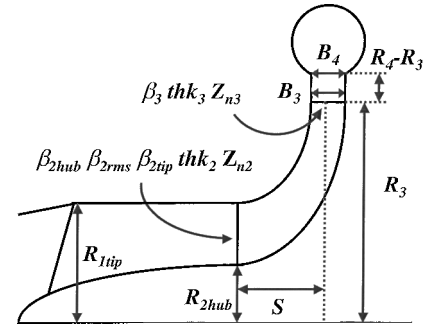

Fig. 12 Design parameters of the multistage pump design problem.

known that nonuniform radial velocity around the periphery of the impeller caused by large slip degrades its head rise. Therefore, this effect should be counted in the future study.

Figure 11 shows the total pressure loss coefficient of the diffusion system of the designs. Pareto-optimal solutions successfully minimize it to increase their total head rise. According to these detailed observations of the results, present MOEA obtained reasonable pareto-optimal solutions, which ensure the feasibility of the present design optimization approach in rocket engine pump designs.

V. Multistage Pump Design

Now, the present method is applied to redesign of the RL10A-3-3A liquid oxygen pump.[24] The RL10A-3-3A engine is a liquid oxygen/liquid hydrogen expander cycle engine, which has been used for the expandable Atlas Centaur upper stage vehicles since 1984. This pump consists of one inducer and a single centrifugal impeller, followed by a vaneless diffuser and conical exit volute.

A. Design Problem Formulation

The objectives are maximization of total head and minimization of input power at the design point, which is shaft rotative speed of 12,900 rpm, total temperature of the fluid entering the pump of −176°C, total pressure of the fluid entering the pump of 28100 kgf/m^2, and mass flow into the pump of 18.1 kg/s. Design parameters and the corresponding parameter ranges are shown in Fig. 12 and Table 3, respectively.

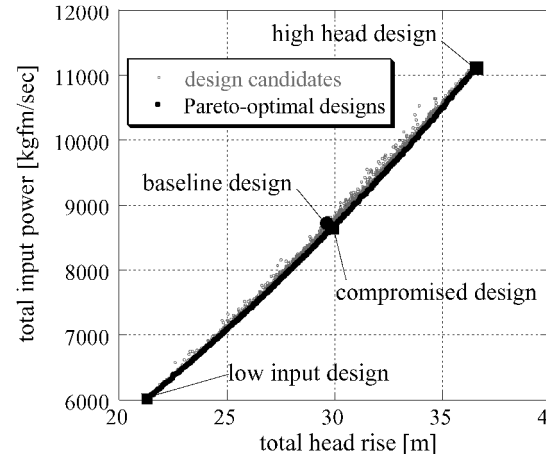

Fig. 13 Objective function values of the multistage pump designs.

B. Results

Based on the discussion in the preceding section, population size and number of generations are set to 120 and 30, respectively. Figure 13 shows total head and input power of pareto-optimal designs, original design, and all other design candidates that have no cavitation. Number of the pareto-optimal designs is 660. Though this design optimization problem involves two stages and a larger number of design parameters, the present MOEA finds reasonable pareto-optimal solutions including some designs that improve both total head and input power by as much as 1%.

Figure 14 shows overall performance maps of the original design and a pareto-optimal design that overcomes the original design in both objectives. The optimal design improves the exit pressure in all

Table 4 Pareto-optimal designs of the multistage pump design problem

First stage							
Design variables	R_{tip}, cm	$R_{2\,hub}$, cm	$\beta_{2\,hub}$, deg	$\beta_{2\,rms}$, deg	$\beta_{2\,tip}$, deg	thk_2, cm	Z_{n2}
High head design	3.00	1.18	49.4	39.3	34.8	0.195	9
Compromised design	2.95	1.27	42.4	37.8	34.1	0.105	8
Low input design	2.97	1.28	42.1	28.5	27.5	0.144	3
Baseline design	2.87	1.22	43.0	27.3	21.6	0.102	3

Second stage							
Design variables	R_3, cm	$(R_4 - R_3)$, cm	B_3, cm	B_4, cm	thk_3, cm	S, cm	Z_{n3}	β_3, deg
High head design	5.59	0.361	0.404	1.04	0.179	2.40	17	87.7
Compromised design	5.46	0.248	0.630	1.12	0.141	2.10	6	66.3
Low input design	5.08	0.194	0.813	0.947	0.0955	2.05	6	64.5
Baseline design	5.33	0.241	0.638	1.02	0.0762	2.23	12	90.0

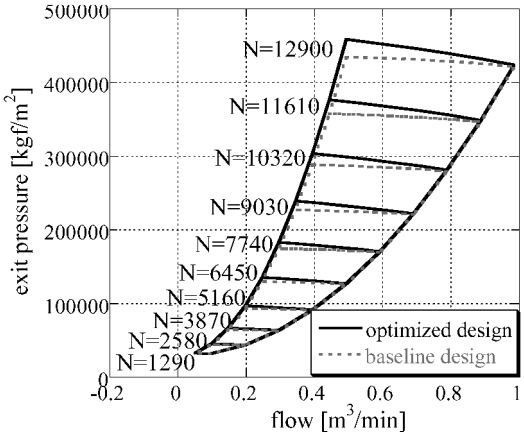

Fig. 14 Multistage pump overall performance map.

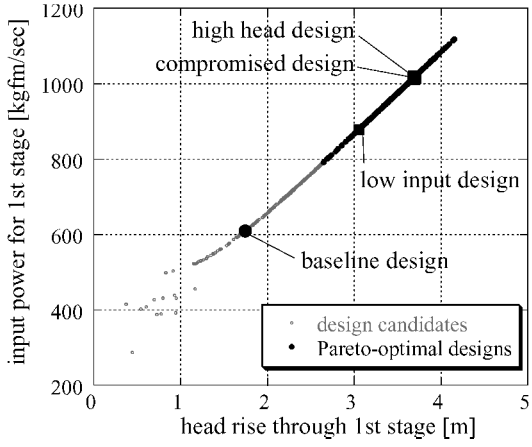

Fig. 15 First-stage performances of the multistage pump designs.

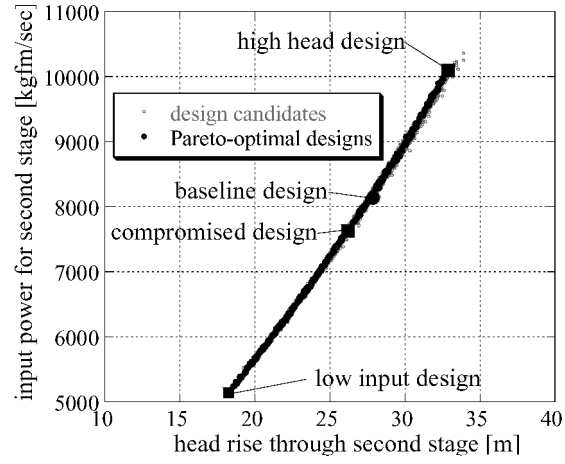

Fig. 16 Second-stage performances of the multistage pump designs.

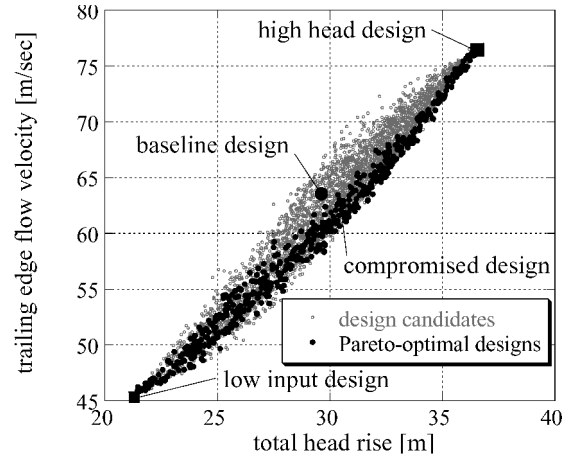

Fig. 17 Flow velocity at second stage exit hub of the multistage pump designs.

off-design conditions. The design parameters of these designs are shown in Table 4.

Figures 15 and 16 illustrate the head rise and the required input power of the first and the second stages. Because the exit of the first stage connects with the inlet of the second stage directly, the relation between the head rise and input power becomes linear. The optimum designs increase their head rise through the first stage because the slope of the curve consisting of pareto-optimal solutions in Fig. 16 is steeper than that of the line in Fig. 15. To increase the head rise through the first stage, the highest head design and the compromised design increase R_{tip} and $\beta_{2\,hub}$. Another interesting thing is that the second stages of the pareto-optimal designs are not optimal by themselves, especially in the high head region. This indicates that each stage of a multistage pump should not be designed separately.

Figure 17 shows fluid velocity at rotor exit hub. This figure is also interesting because the pareto-optimal designs in the high total head region have smaller fluid velocity at exit like the single-stage pump design, whereas the pareto-optimal designs in the low total head region do not necessarily have small fluid velocity at exit. This is probably because of complicated interactions between the first and second stages.

Figure 18 is the total pressure loss coefficient of the designs. The optimal designs in the high total head region maximize their total pressure loss coefficient, but the optimal designs in the low total head region minimize it. More work is necessary to understand the multistage pump designs.

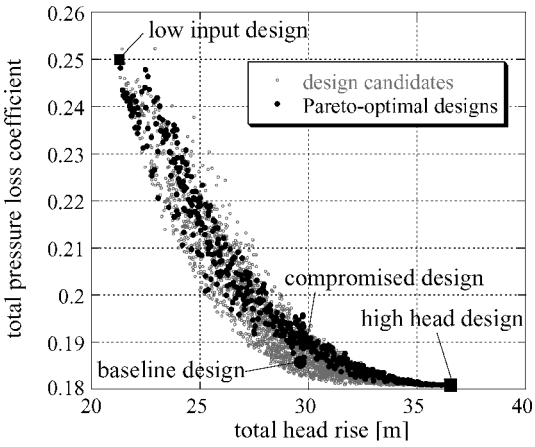

Fig. 18 Total pressure loss coefficient of the multistage pump designs.

VI. Conclusions

In the present study a design optimization method for cryogenic rocket engine turbopumps has been developed. A multiobjective evolutionary algorithm is used for the multiobjective optimization of pump designs. Performances of design candidates are evaluated by using the meanline pump flow modeling method, which is based on the Euler turbine equation coupled with empirical correlations for rotor efficiency.

To demonstrate the feasibility of the present approach, single-stage centrifugal pump design and multistage pump design optimizations were demonstrated. The number of pump performance evaluations necessary to obtain a reasonable pareto-optimal set for the conceptual rocket engine pump design was investigated using the single-stage centrifugal pump design optimization. In both cases the present method obtained reasonable pareto-optimal solutions that include designs outperforming the original design in total head as well as input power by 1%. Detailed observation of the design results also revealed some important design policies in turbopump design of cryogenic rocket engines. These results ensured the feasibility of EA-based design optimization method in this field.

Acknowledgment

The authors would like to thank J. Veres of NASA Glenn Research Center for providing the pump code.

References

[1]Stewart, T. J., "A Critical Survey on the Status of Multiple Criteria Decision Making and Practice," *International Journal of Management Science*, Vol. 20, No. 5/6, 1992, pp. 569–586.

[2]Hicks, R. M., Murman, E. M., and Vanderplaats, G. N., "An Assessment of Airfoil Design by Numerical Optimization," NASA TM X-3092, July 1974.

[3]William, H. P., Saul, A. T., William, T. V., and Brian, P. F., *Numerical Recipes in Fortran 77: The Art of Scientific Computing*, Cambridge Univ. Press, Cambridge, England, U.K., 1996, pp. 436–448.

[4]Quagliarella, D., Periaux, J., Poloni, C., and Winter, G. (eds.), *Genetic Algorithms in Engineering and Computer Science*, Wiley, New York, 1997.

[5]Powell, D. J., Tong, S. S., and Sholbick, M. M., "EnGENEous Domain Independent, Machine Learning for Design Optimization," *Proceedings of the Third International Conference on Genetic Algorithms*, Morgan Kaufmann, San Mateo, CA, 1989, pp. 151–159.

[6]Obayashi, S., and Takanashi, S., "Genetic Optimization of Target Pressure Distributions for Inverse Design Methods," *AIAA Journal*, Vol. 34, No. 5, 1996, pp. 881–886.

[7]Oyama, A., "Multidisciplinary Optimization of Transonic Wing Design Based on Evolutionary Algorithms Coupled with CFD Solver," *Proceedings of the European Congress on Computational Methods in Applied Sciences and Engineering* [CD-ROM], CIMNE, Barcelona, Spain, 2000.

[8]Sasaki, D., Obayashi, S., Sawada, K., and Himeno, R., "Multiobjective Aerodynamic Optimization of Supersonic Wings Using Navier–Stokes Equations," *Proceedings of the European Congress on Computational Methods in Applied Sciences and Engineering* [CD-ROM], CIMNE, Barcelona, Spain, 2000.

[9]Fonseca, C. M., and Fleming, P. J., "Genetic Algorithms for Multiobjective Optimization: Formulation, Discussion and Generalization," *Proceedings of the Fifth International Conference on Genetic Algorithms*, Morgan Kaufmann, San Mateo, CA, 1993, pp. 416–423.

[10]Tsutsui, S., and Fujimoto, Y., "Forking Genetic Algorithms with Blocking and Shrinking Modes (fGA)," *Proceedings of the Fifth International Conference on Genetic Algorithms*, Morgan Kaufmann, San Mateo, CA, 1993, pp. 206–213.

[11]Goldberg, D. E., *Genetic Algorithms in Search, Optimization and Machine Learning*, Addison Wesley Longman, Reading, MA, 1989, pp. 191–195.

[12]Eshelman, L. J., and Schaffer, J. D., "Real-Coded Genetic Algorithms and Interval Schemata," *Foundations of Genetic Algorithm 2*, Morgan Kaufmann, San Mateo, CA, 1993, pp. 187–202.

[13]Booker, L. B., "Improving Search in Genetic Algorithms," *Genetic Algorithms and Simulated Annealing*, Morgan Kaufmann, San Mateo, CA, 1987, pp. 61–73.

[14]Veres, J. P., "Centrifugal and Axial Pump Design and Off-Design Performance Prediction," NASA TM 106745, Oct. 1994.

[15]Kovats, A., *Design and Performance of Centrifugal and Axial Flow Pumps and Compressors*, Macmillan, New York, 1964, pp. 362, 363, 30–34.

[16]Stepanoff, A. J., *Centrifugal and Axial Flow Pumps: Theory, Design, and Applications,* Wiley, New York, 1957, pp. 73–76.

[17]Fowler, J. R., "GASPLUS User's Manual," National Air Space Plane CR 1012, March 1988.

[18]Brunner, J. J., "M-1 Oxidizer Scale Pump Performance with Initial and Interim Design Impellers," Aerojet General Corp., Rept. Number TPR 0047, Contract NAS3-2555, Sacramento, CA, April 1966.

[19]Fonseca, C. M., and Fleming, P. J., "On the Performance Assessment and Comparison of Stochastic Multiobjective Optimizers," *Parallel Problem Solving from Nature—PPSN IV, Lecture Notes in Computer Science,* edited by H. M. Voigt, W. Ebeling, I. Rechenberg, and H. P. Schwefel, Springer-Verlag, Berlin, 1996, pp. 584–593.

[20]Van Veldhuizen, D. A., and Gary, B. L., "Multiobjective Evolutionary Algorithm Test Suites," *Proceedings of the 1999 ACM Symposium on Applied Computing*, ACM Press, New York, 1999, pp. 351–357.

[21]Zitzler, E., Deb, K., and Thiele, L., "Comparison of Multiobjective Evolutionary Algorithms: Empirical Results," *Evolutionary Computation Journal*, Vol. 8, No. 2, 2000, pp. 173–195.

[22]Knowles, J. D., Corne, D. W., and Oates, M. J., "On the Assessment of Multiobjective Approaches to the Adaptive Distributed Database Management Problem," *Parallel Problem Solving from Nature—PPSN VI, Lecture Notes in Computer Science*, edited by M. Schoenauer, K. Deb, G. Rudolph, X. Yao, E. Lutton, J. J. Merelo, and H. P. Schwefel, Springer-Verlag, Berlin, 1996, pp. 869–878.

[23]Van Veldhuizen, D. A., and Gary, B. L., "Evolutionary Computation and Convergence to a Pareto Front," *Late Breaking Papers at the Genetic Programming 1998 Conference*, edited by John R. Koza, Stanford Univ., Stanford, CA, 1998, pp. 221–228.

[24]Binder, M., Tomsik, T., and Veres, J. P., "RL10A-3-3A Rocket Engine Modeling Project," NASA TM 107318, Jan. 1997.